

The Color Dipole Picture¹

Dieter Schildknecht

*Fakultät für Physik, Universität Bielefeld,
Universitätsstraße 25, 33615 Bielefeld, Germany*
and

*Max-Planck-Institute for Physics, Föhringer Ring 6,
80805 Munich, Germany*

Abstract. We give a brief exposition of the color dipole picture of deep inelastic scattering.

Keywords: Deep inelastic scattering, color transparency, saturation.

PACS: 10 , 12.38.-t , 12.40.Vv , 13.60.Hb

INTRODUCTION

In Fig. 1 [1], I show² the experimental data for the proton electromagnetic structure function $F_2(x, Q^2)$ as a function of $1/W^2$, and, for comparison, as a function of the Bjorken variable $x = Q^2/(W^2 + Q^2 - M^2) \simeq Q^2/W^2$ (for $x \ll 0.1$). For photon virtualities of $10 \text{ GeV}^2 \leq Q^2 \leq 100 \text{ GeV}^2$, and for the photon-proton center of mass energy, W , sufficiently large, we observe a simple scaling behavior $F_2(x, Q^2) = F_2(W^2)$. The theoretical curve [1] in Fig. 1 is based on $F_2(W^2) = f_2(W^2/1 \text{ GeV}^2)^{C_2}$,

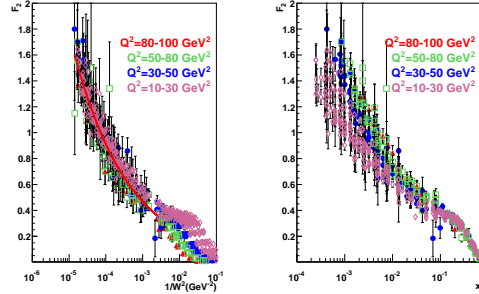


Figure 1: The structure function $F_2(x, Q^2)$.

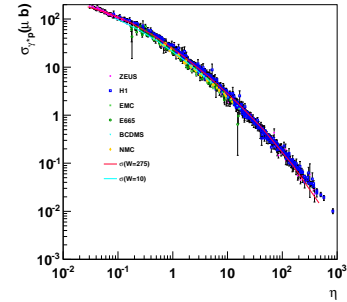


Figure 2: Scaling [4, 5] of $\sigma_{\gamma^*p}(W^2, Q^2) = \sigma_{\gamma^*p}(\eta(W^2, Q^2))$.

where $f_2 = 0.063$ and $C_2 = 0.29$. In terms of the photoabsorption cross section,

¹Presented at Diffraction 2012, Lanzarote, Canary Islands (Spain), September 10-15, 2012 (Proceedings to appear)

²For a more elaborate presentation of the color dipole picture and a more complete list of references compare also the recent review papers in refs. [2] and [3].

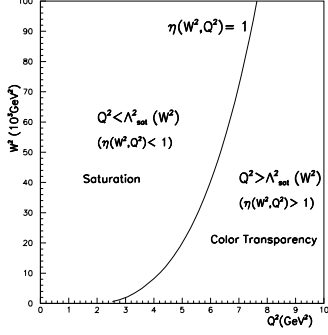


Figure 3: The (Q^2, W^2) plane.

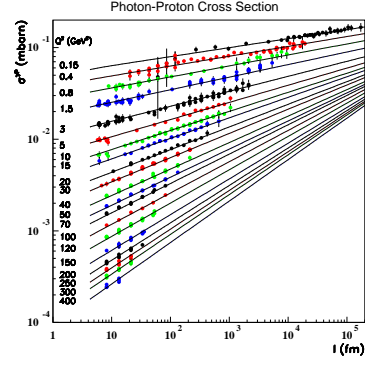


Figure 4: The Caldwell fit[6].

$\sigma_{\gamma^*p}(W^2, Q^2) \simeq (4\pi^2\alpha/Q^2)F_2(x, Q^2)$, upon introducing [4] the low-x scaling variable

$$\eta(W^2, Q^2) = \frac{Q^2 + m_0^2}{\Lambda_{sat}^2(W^2)}, \quad (1)$$

where $m_0^2 \cong 0.15 \text{ GeV}^2$ and $\Lambda_{sat}^2(W^2) \sim (W^2/1 \text{ GeV}^2)^{C_2}$, one finds scaling [4, 5] in an extended region that includes the transition to $Q^2 \rightarrow 0$. Compare Fig. 2. From Fig. 2, we read off the functional dependence of,

$$\sigma_{\gamma^*p}(W^2, Q^2) = \sigma_{\gamma^*p}(\eta(W^2, Q^2)) \sim \sigma^{(\infty)} \begin{cases} \frac{1}{\eta(W^2, Q^2)}, & \text{for } (\eta(W^2, Q^2) \gg 1), \\ \ln \frac{1}{\eta(W^2, Q^2)}, & \text{for } (\eta(W^2, Q^2) \ll 1), \end{cases} \quad (2)$$

where the cross section $\sigma^{(\infty)}$ is at most very weakly dependent on the energy W .

The (Q^2, W^2) plane corresponding to the behavior in Fig. 2 is simple, compare Fig. 3. The logarithmic dependence in (2) implies the transition from the $1/\eta(W^2, Q^2)$ dependence of “color transparency” to the Q^2 -independent “saturation” limit that coincides [4, 5] with $Q^2 = 0$ photoproduction

$$\lim_{\substack{W^2 \rightarrow \infty \\ Q^2 \text{ fixed}}} \frac{\sigma_{\gamma^*p}(\eta(W^2, Q^2))}{\sigma_{\gamma^*p}(\eta(W^2, Q^2 = 0))} = \lim_{\substack{W^2 \rightarrow \infty \\ Q^2 \text{ fixed}}} \frac{\ln \left(\frac{\Lambda_{sat}^2(W^2)}{m_0^2} \frac{m_0^2}{(Q^2 + m_0^2)} \right)}{\ln \frac{\Lambda_{sat}^2(W^2)}{m_0^2}} = 1 + \lim_{\substack{W^2 \rightarrow \infty \\ Q^2 \text{ fixed}}} \frac{\ln \frac{m_0^2}{Q^2 + m_0^2}}{\ln \frac{\Lambda_{sat}^2(W^2)}{m_0^2}} = 1. \quad (3)$$

The approach to a Q^2 -independent limit for $W^2 \rightarrow \infty$ at Q^2 fixed was recently also observed by Caldwell [6], compare Fig. 4, showing the empirical fit of $\sigma_{\gamma^*p}(W^2, Q^2) = \sigma_0(Q^2)(W^2/2M_pQ^2)^{\lambda_{eff}(Q^2)}$.

In what follows, I shall point out that not only the existence of scaling in $\eta(W^2, Q^2)$, but the specific dependence on $\eta(W^2, Q^2)$ in (2) as well, both are unique and general model-independent consequences from the color dipole picture (CDP).

THE COLOR DIPOLE PICTURE: MODEL-INDEPENDENT CONCLUSIONS

At low values of $x \ll 0.1$, deep inelastic scattering proceeds via interaction of long-lived quark-antiquark, $q\bar{q}$, fluctuations of the (virtual) photon that interact with the gluon field in the nucleon. The total photoabsorption cross section is given by [7, 8, 4, 5, 1]

$$\begin{aligned} \sigma_{\gamma_{L,T}^*}(W^2, Q^2) &= \int dz \int d^2\vec{r}_\perp |\psi_{L,T}(\vec{r}_\perp, z(1-z), Q^2)|^2 \sigma_{(q\bar{q})p}(\vec{r}_\perp, z(1-z), W^2) = \\ &= \frac{\alpha}{\pi} \sum_q Q_q^2 Q^2 \int dr'_\perp K_{0,1}^2(r'_\perp Q) \sigma_{(q\bar{q})_{L,T}^{J=1}p}(r'^2_\perp, W^2). \end{aligned} \quad (4)$$

In the second step in (4), the explicit form of the square of the ‘‘photon wave function’’ $|\psi_{L,T}(\vec{r}_\perp, z(1-z), Q^2)|^2$ for massless quarks in terms of the modified Bessel functions $K_{0,1}^2(r'_\perp Q^2)$ was inserted, and a $J = 1$ partial wave projection of the $(q\bar{q})p$ dipole cross section was performed. The transverse size \vec{r}'_\perp of the $(q\bar{q})^{J=1}$ dipole states is related to the transverse size \vec{r}_\perp via $\vec{r}'_\perp = \vec{r}_\perp \sqrt{z(1-z)}$ with $0 \leq z \leq 1$ denoting the quark longitudinal momentum fraction of the photon transition to $q\bar{q}$ pairs. The sum over the active quark charges squared in (4) is denoted by $\sum_q Q_q^2$.

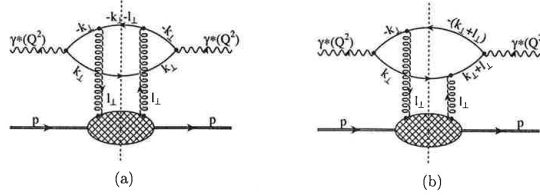


Figure 5: Two of the four diagrams for the $q\bar{q}$ dipole interaction.

Two of the four contributing diagrams for the $q\bar{q}$ interaction with the gluons in the nucleon are shown in Fig. 5. The color-gauge invariant two-gluon interaction, as a consequence of the two diagrams in Fig. 5, implies a representation of the $(q\bar{q})_{L,T}^{J=1}p$ cross section of the form (e.g. ref. [1])

$$\sigma_{(q\bar{q})_{L,T}^{J=1}p}(r'_\perp, W^2) = \pi \int d\vec{l}'_\perp \bar{\sigma}_{(q\bar{q})_{L,T}^{J=1}p}(\vec{l}'^2_\perp, W^2) \left(1 - \frac{\int d\vec{l}'_\perp \bar{\sigma}_{(q\bar{q})_{L,T}^{J=1}p}(\vec{l}'^2_\perp, W^2) J_0(l'_\perp r'_\perp)}{\int d\vec{l}'_\perp \bar{\sigma}_{(q\bar{q})_{L,T}^{J=1}p}(\vec{l}'^2_\perp, W^2)} \right), \quad (5)$$

where $J_0(l'_\perp r'_\perp)$ denotes the Bessel function with index 0. At any fixed size r'_\perp , we assume the dominant contribution to the integrals in (5) to be due to a restricted range of $r'_\perp l'_\perp \leq r'_\perp l'_{\perp Max}(W^2)$, with $l'_{\perp Max}$ increasing with W^2 . Inspection of the integral in (5) for fixed r'_\perp as a function of W^2 , reveals two different limits for the dipole cross section on the left-hand side. There is either ‘‘color transparency’’, $\sigma_{(q\bar{q})_{L,T}^{J=1}p}(r'_\perp, W^2) \sim r'^2_\perp$ or else, ‘‘saturation’’ corresponding to the r'_\perp -independent limit of $\sigma_{L,T}^{(\infty)}(W^2) = \pi \int d\vec{l}'_\perp \bar{\sigma}_{(q\bar{q})_{L,T}^{J=1}p}(\vec{l}'^2_\perp, W^2)$. As a consequence of the strong fall-off of

the modified Bessel functions in (4), the color transparency and saturation limits of the dipole cross section translate into two different limits of the photoabsorption cross section that are given by

$$\sigma_{\gamma^*p}(W^2, Q^2) = \sigma_{\gamma^*p}(\eta(W^2, Q^2)) = \frac{\alpha}{\pi} \sum_q Q_q^2 \cdot \begin{cases} \frac{1}{6}(1+2\rho)\sigma^{(\infty)} \frac{1}{\eta(W^2, Q^2)}, \\ \sigma^{(\infty)} \ln \frac{1}{\eta(W^2, Q^2)}, \end{cases} \quad (6)$$

where the upper and the lower line on the right hand side in (6) refer to $\eta(W^2, Q^2) \gg 1$ and $\eta(W^2, Q^2) \ll 1$, respectively. The result (6) from the CDP coincides with the experimental one (2). In (6), the ‘‘saturation scale’’, $\Lambda_{sat}^2(W^2)$ from (1), is an increasing function of W^2 that is given by $\Lambda_{sat}^2(W^2) = (\pi/\sigma_L^{(\infty)}) \int d\vec{l}_\perp^2 d\vec{l}'_\perp^2 \bar{\sigma}_{(q\bar{q})L=1p}(\vec{l}_\perp^2, W^2)$, and ρ is related to the longitudinal-to-transverse ratio R given by $R = 1/2\rho$ at sufficiently large Q^2 , with $\rho = 4/3$ [9, 1] due to the different size of longitudinally-versus-transversely polarized $q\bar{q}$ states.

CONNECTION WITH THE PQCD-IMPROVED PARTON MODEL

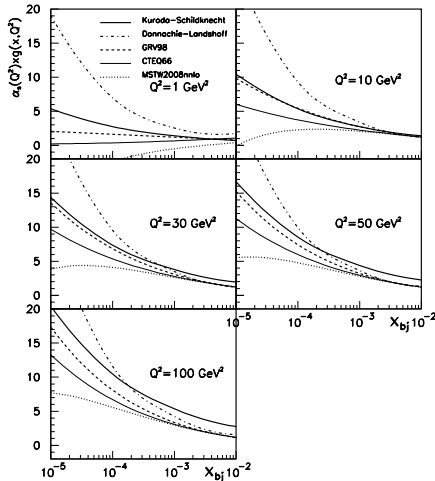


Figure 6: The gluon distribution function (8) compared with the results from the hard Pomeron part of a Regge fit [11] and from several global pQCD fits [12] to $F_2(x, Q^2)$.

Requiring consistency of the CDP with the pQCD-improved parton model, in particular, requiring consistency with the evolution equation for the structure function $F_2(x, Q^2) \sim (W^2)^{C_2}$, as shown in Fig. 1, one finds a simple explicit relation for the exponent C_2 that is given by [10, 1]

$$C_2 = \frac{1}{2\rho + 1} \left(\frac{\xi_2}{\xi_L} \right)^{C_2} = 0.29. \quad (7)$$

The value of $C_2 = 0.29$ is consistent with the experimental results in Figs. 1 and 2. In (7) the previously mentioned predicted value of $\rho = 4/3$ was inserted. The sensitivity on the rescaling factors in the relevant interval of $1 \leq \xi_2/\xi_L \leq 1.5$ is fairly weak, implying $0.27 \leq C_2 \leq 0.31$. The effective gluon distribution in Fig. 6 [1] based on

$$\alpha_s(Q^2)G(x, Q^2) = \frac{3\pi}{\sum_q Q_q^2(2\rho + 1)} \frac{f_2}{\xi_L^{C_2=0.29}} \left(\frac{W^2}{1 \text{ GeV}^2} \right)^{C_2=0.29}. \quad (8)$$

is consistent with the widely varying results from the literature.

THE COLOR DIPOLE PICTURE: MODEL-DEPENDENT PARAMETERIZATION

Any specific ansatz for the dipole cross section has to interpolate the general model-independent functional dependences in (6). For details we have to refer to refs. [4, 5, 1] and restrict ourselves to showing the comparison [1] with experiment in Figs. 7 and 8.

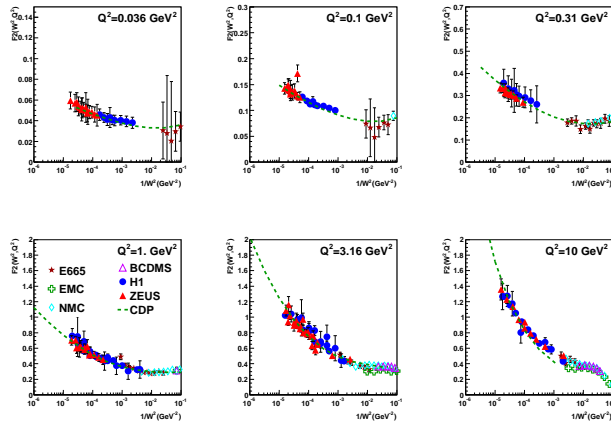


Figure 7: The predictions from the CDP [1] for the structure function $F_2(W^2, Q^2)$ compared with the experimental data for $0.036 \leq Q^2 \leq 10 \text{ GeV}^2$.

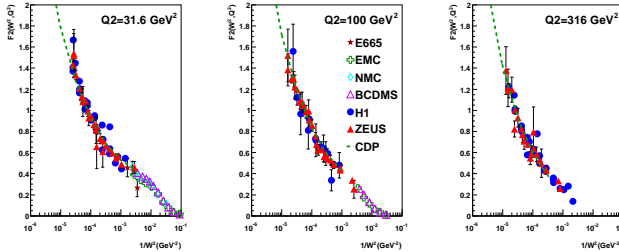


Figure 8: As in Fig. 7, but for $31.6 \text{ GeV}^2 \leq Q^2 \leq 316 \text{ GeV}^2$.

CONCLUSIONS

Scaling in $\eta(W^2, Q^2)$ of the total photoabsorption cross section, as well as the specific functional dependences on $\eta(W^2, Q^2)$, corresponding to either color transparency or saturation, have been recognized as general consequences from the color-gauge-invariant interaction of dipole fluctuations of the photon, $\gamma^* \rightarrow q\bar{q}$, with the gluon field in the nucleon. Color transparency corresponds to cancellation between the two interaction channels related to the two diagrams in Fig. 5. The vanishing of this cancellation in

the high-energy limit of $W^2 \rightarrow \infty$ at any fixed value of Q^2 implies saturation of the cross section to the photoproduction limit.

ACKNOWLEDGMENTS

Many thanks to Roberto Fiore, Alessandro Papa and Agustin Sabio Vera for the invitation to Diffraction 2012 and the efficient organization of a very successful workshop in the beautiful surroundings of Lanzarote.

References

- [1] M. Kuroda and D. Schildknecht, Phys. Rev. **D85** (2012) 094001.
- [2] D. Schildknecht, Invited Talk, Ringberg Workshop on New Trends in HERA Physics, Ringberg Castle, September 25-28, 2011, Nucl. Phys. B, Proc. Supplement **222-224** (2012) 108.
- [3] D. Schildknecht, Invited Talk, 50th International School of Subnuclear Physics, Erice, Italy, June 23 - July 2, 2012, arXiv: 1210.0733v1 [hep-ph], to appear in Proceedings (World Scientific)
- [4] D. Schildknecht, in Diffraction 2000, Cetraro, Italy, September 2-7, 2000, Nucl. Phys. B, Proc. Supplement **99** (2001) 121;
D. Schildknecht, B. Surrow, M. Tentyukov, Phys. Lett. **B499** (2001) 116;
G. Cvetič, D. Schildknecht, B. Surrow, M. Tentyukov, EPJC **20** (2001) 77.
- [5] D. Schildknecht, in DIS 2001, The 9th International Workshop on Deep Inelastic Scattering, Bologna, Italy, 2001, G. Brassi et al. (Eds.), World Scientific, Singapore, 2002, p. 798;
D. Schildknecht, B. Surrow and M. Tentyukov, Mod. Phys. Lett. **A16** (2001) 1829.
- [6] A. Caldwell, [arXiv:0802.0769]
- [7] N.N. Nikolaev, B.G. Zakharov, Z. Phys. C49, 607 (1991).
- [8] G. Cvetič, D. Schildknecht, A. Shoshi, Eur. Phys. J **C13** (2000) 301.
- [9] M. Kuroda and D. Schildknecht, Phys. Lett. **B670** (2008) 129.
- [10] M. Kuroda and D. Schildknecht, Phys. Lett. **B618** (2005) 84.
- [11] A. Donnachie and P. Landshoff, Phys. Lett. **B533** (2002) 277.
- [12] Durham Data Base, <http://durpdg.dur.ac.uk/HEPDATA/PDF>